

This copy is for your personal, non-commercial use only.

If you wish to distribute this article to others, you can order high-quality copies for your colleagues, clients, or customers by [clicking here](#).

Permission to republish or repurpose articles or portions of articles can be obtained by following the guidelines [here](#).

The following resources related to this article are available online at www.sciencemag.org (this information is current as of May 5, 2010):

Updated information and services, including high-resolution figures, can be found in the online version of this article at:

<http://www.sciencemag.org/cgi/content/full/321/5889/680>

Supporting Online Material can be found at:

<http://www.sciencemag.org/cgi/content/full/1157707/DC1>

A list of selected additional articles on the Science Web sites **related to this article** can be found at:

<http://www.sciencemag.org/cgi/content/full/321/5889/680#related-content>

This article **cites 30 articles**, 5 of which can be accessed for free:

<http://www.sciencemag.org/cgi/content/full/321/5889/680#otherarticles>

This article has been **cited by** 15 article(s) on the ISI Web of Science.

This article has been **cited by** 8 articles hosted by HighWire Press; see:

<http://www.sciencemag.org/cgi/content/full/321/5889/680#otherarticles>

This article appears in the following **subject collections**:

Atmospheric Science

<http://www.sciencemag.org/cgi/collection/atmos>

24. R. J. Cava, E. A. Rietman, *Phys. Rev. B* **30**, 6896 (1984).
 25. C. Ohly, S. Hoffmann-Eifert, X. Guo, *J. Am. Ceram. Soc.* **89**, 2845 (2006).
 26. A. Peters, C. Korte, D. Hesse, N. Zakharov, J. Janek, *Solid State Ionics* **178**, 67 (2007).
 27. D. J. Wallis, N. D. Browning, *J. Am. Ceram. Soc.* **80**, 781 (1997).
 28. W. Siemons *et al.*, *Phys. Rev. Lett.* **98**, 196802 (2007).
 29. A. Kalabukhov *et al.*, *Phys. Rev. B* **75**, 121404(R) (2007).
 30. K. L. Ngai, A. K. Rizos, *Phys. Rev. Lett.* **76**, 1296 (1996).
 31. K. L. Ngai, G. N. Greaves, C. T. Moyhian, *Phys. Rev. Lett.* **80**, 1018 (1998).
 32. W. K. Lee, J. F. Liu, A. S. Nowick, *Phys. Rev. Lett.* **67**, 1559 (1991).
 33. K. L. Ngai, *J. Chem. Phys.* **110**, 10576 (1999).
 34. J. Habasaki, K. L. Ngai, Y. Hiwatari, *J. Chem. Phys.* **120**, 8195 (2004).
 35. J. Fleig, H. L. Tuller, J. Maier, *Solid State Ionics* **174**, 261 (2004).
 36. This work was supported by grants from the Spanish Ministry for Science and Innovation (MAT2005 06024, MAT2007 62162, and MAT 2008) and by the Madrid Regional Government Comunidad Autónoma de Madrid through Universidad Complutense de Madrid Groups Programme. We thank U. Complutense—Centro de Asistencia a la Investigación de Técnicas Físicas for technical support. Research at Oak Ridge National Laboratory (M.V. and S.J.P.) was sponsored by the Division

of Materials Sciences and Engineering of the U.S. Department of Energy. We are grateful to J. T. Luck for help with STEM specimen preparation and to F. de Andrés for help with the graphic design of the hard spheres model.

Supporting Online Material

www.sciencemag.org/cgi/content/full/321/5889/676/DC1
 Materials and Methods
 SOM Text
 Figs. S1 to S3
 References

12 February 2008; accepted 13 June 2008
 10.1126/science.1156393

High-Resolution Greenland Ice Core Data Show Abrupt Climate Change Happens in Few Years

Jørgen Peder Steffensen,^{1*} Katrine K. Andersen,¹ Matthias Bigler,^{1,2} Henrik B. Clausen,¹ Dorthe Dahl-Jensen,¹ Hubertus Fischer,^{2,3} Kumiko Goto-Azuma,⁴ Margareta Hansson,⁵ Sigfús J. Johnsen,¹ Jean Jouzel,⁶ Valérie Masson-Delmotte,⁶ Trevor Popp,⁷ Sune O. Rasmussen,¹ Regine Röthlisberger,^{2,8} Urs Ruth,³ Bernhard Stauffer,² Marie-Louise Siggaard-Andersen,¹ Árný E. Sveinbjörnsdóttir,⁹ Anders Svensson,¹ James W. C. White⁷

The last two abrupt warmings at the onset of our present warm interglacial period, interrupted by the Younger Dryas cooling event, were investigated at high temporal resolution from the North Greenland Ice Core Project ice core. The deuterium excess, a proxy of Greenland precipitation moisture source, switched mode within 1 to 3 years over these transitions and initiated a more gradual change (over 50 years) of the Greenland air temperature, as recorded by stable water isotopes. The onsets of both abrupt Greenland warmings were slightly preceded by decreasing Greenland dust deposition, reflecting the wetting of Asian deserts. A northern shift of the Intertropical Convergence Zone could be the trigger of these abrupt shifts of Northern Hemisphere atmospheric circulation, resulting in changes of 2 to 4 kelvin in Greenland moisture source temperature from one year to the next.

Ice core records from Greenland have been instrumental in investigating past abrupt climate change. As compared with other sedimentary records, the ice core records have unparalleled temporal resolution and continuity (1–3). The newest Greenland ice core, from the North Greenland Ice Core Project (NGRIP), has been measured at very high resolution for water isotope

ratios, dust, and impurity concentrations. This allows researchers for the first time to follow the ice core proxies of Greenland temperature, accumulation, moisture origin, and aerosol deposition at subannual resolution over the very abrupt climate changes in the period from 15.5 to 11.0 thousand years ago (ka) (measured from 2000 AD throughout this study).

In the Northern Hemisphere, the last glacial period ended in a climatic oscillation composed of two abrupt warmings interrupted by one cooling event (3–6). The temperature changed rapidly from glacial to mild conditions in the Bølling and Allerød periods and then returned to glacial values in the Younger Dryas period before the onset of the present warm interglacial, the Holocene (Fig. 1, and see table S1 for classification of climate periods). The shape and duration of the abrupt climate change at the termination of the last glacial have previously been constrained by Greenland ice core records from DYE-3 (4, 7), Greenland Ice Core Project (GRIP) (8) and Greenland Ice Sheet Project 2 (GISP2) (3, 6, 9), but sampling of these cores did not typically achieve a resolution sufficient to resolve annual layers. Because of new continuous flow analysis

(CFA) systems (10–12), impurity and chemical records of the recent NGRIP ice core (1) have been obtained at subannual resolution, which allows for the multiple-proxy identification of annual-layer thickness and the construction of a new Greenland time scale, the Greenland Ice Core Chronology 2005 (GICC05) (2). Complementary highly detailed stable water isotope profiles ($\delta^{18}\text{O}$ and δD) have been measured on the NGRIP ice core covering the period from 15.5 to 11.0 ka at 2.5-to-5.0-cm resolution, corresponding to one to three samples per year. They were compared with the concentrations of insoluble dust, soluble sodium (Na^+), and calcium (Ca^{2+}), each measured with CFA at subannual resolution (10, 12, 13) (Fig. 2) and, when available, with the highest-resolution data from GRIP, GISP2, and DYE-3 ice cores on the GICC05 time scale.

Across the warming transitions, the records exhibit clear shifts between two climate states. We characterize a shift to be significant if the mean values of the climate states on each side of the shift differ by more than the statistical standard error of the noise of a 150-year period of these climate states. A simple but objective approach to finding the best timing of the transition is to characterize the shift observed in each proxy as a “ramp”: a linear change from one stable state to another. We applied a ramp-fitting method (14) to determine the timing of the transitions. The method entails using weighted least-squares regression to determine the ramp location and a bootstrap simulation to estimate the uncertainty of the results [transition times are listed in Table 1; see supporting online material (SOM) methods and table S2 for more detailed information on the method and the ramp fit values and uncertainties (15)]. Data and fitted ramps are shown in Figs. 2 and 3. For annual layer thickness (λ), concentrations of dust, Ca^{2+} , and Na^+ , logarithmic scales were used because these proxies are approximately log-normally distributed.

The $\delta^{18}\text{O}$ record is a proxy for past air temperature at the ice core site (16, 17). Although the magnitude of Greenland $\delta^{18}\text{O}$ changes can be influenced by changing site and source temperatures and by snowfall seasonality (16, 18, 19), the timing of $\delta^{18}\text{O}$ changes is dominated by the changing site temperature (18). The $\delta^{18}\text{O}$ warming transition at 14.7 ka was the most rapid and occurred within a remarkable 3 years, whereas the

¹Centre for Ice and Climate, Niels Bohr Institute, University of Copenhagen, Juliane Maries Vej 30, DK-2100 Copenhagen OE, Denmark.

²Climate and Environmental Physics, Physics Institute, University of Bern, Sidlerstrasse 5, CH-3012, Switzerland.

³Alfred-Wegener-Institute for Polar- and Marine Research (AWI), Postfach 120161, D-27515 Bremerhaven, Germany.

⁴National Institute of Polar Research, Kaga 1-9-10, Itabashi-ku, Tokyo 173-8515, Japan.

⁵Department of Physical Geography and Quaternary Geology, Stockholm University, S-106 91, Stockholm, Sweden.

⁶Institut Pierre Simon Laplace/Laboratoire des Sciences du Climat et de l'Environnement, Commissariat à l'Énergie Atomique (CEA)—CNRS—Université de Versailles Saint Quentin en Yvelines, CEA Saclay, 91191 Gif-Sur-Yvette, France.

⁷The Institute of Arctic and Alpine Research, Campus Box 450, University of Colorado, Boulder, CO 80309-0450, USA.

⁸British Antarctic Survey, Natural Environment Research Council, High Cross, Madingley Road, Cambridge CB3 0ET, UK.

⁹Raunvísindastofnun Háskólans, Dunhagi 3, Iceland.

*To whom correspondence should be addressed. E-mail: jps@gfy.ku.dk

warming transition at 11.7 ka lasted 60 years; both correspond to a warming of more than 10 K (6, 20). $\delta^{18}\text{O}$ records from the GRIP (9, 21), GISP2 (9), and DYE-3 (7, 17) ice cores across the 11.7 ka transition show a similar duration. The $\delta^{18}\text{O}$ cooling transition at 12.9 ka lasted more than two centuries, much longer than the warming transitions, and does not meet the above criteria for being described as a ramp shift.

Annual layer thickness λ (estimated independently of $\delta^{18}\text{O}$ by annual layer counting) increased by 40% during the two warmings over 3 and 40 years, respectively. During the cooling, λ decreased by 33% over a period of 152 years. When corrected for strain, λ represents the annual precipitation rate, which is linked to site temperature and to synoptic weather patterns. Both Greenland site temperature and accumulation are expected to be strongly related to the extent of the northern sea ice (22).

The most abrupt transitions are those of the deuterium excess $d = \delta\text{D} - 8\delta^{18}\text{O}$, a second-order isotopic parameter that contains information on fractionation effects caused by the evaporation of source water (16, 18, 23). The excess is considered to be mainly a proxy of past ocean surface temperatures at the moisture-source region (16, 18, 23). Our dust record, not showing a similar abrupt transition as the excess, rules out the alternative explanation, that a rapid shift in d was linked with changes in cloud condensation nuclei and kinetic fractionation taking place during cloud ice-crystal formation (24, 25). The excess record shows a 2 to 3 per mil (‰) decrease in d during the warmings, corresponding to a cooling by 2 to 4 K of the marine moisture-source region (16, 18) over 1 to 3 years, and a 2 to 3‰ increase during the cooling transition. Figure 3 presents the rapid changes of d on a more highly resolved time axis in order to clearly

show the rapid change between the climate states. The moisture-source evaporation conditions can change either because of a shift in atmospheric circulation, resulting in relocation of the moisture source, or because of changing sea surface temperature, humidity, or wind conditions at a stationary moisture source. The extremely rapid shifts in both warmings and coolings rule out an explanation that is purely in terms of sea-ice extent, because the northern sea ice extended far south during the final phase of the cold stadials and is not expected to have broken down in just 1 to 3 years (26, 27). Finally, if d was reflecting only changes in weather pattern trajectories with respect to the NGRIP observation point, then it would be expected to detect simultaneous changes in other parameters, such as dust, Ca^{2+} , and λ , which is not the case. Thus, we interpret the rapid shifts in d to be more likely a consequence of changed source regions of the water vapor reaching Greenland. This points to a reorganization of atmospheric circulation from one year to the next.

The concentrations of insoluble dust and Ca^{2+} reflect both source strength and transport conditions from terrestrial sources, which for Greenland are the low-latitude Asian deserts (10, 28). At the two warming events, the concentrations of dust and Ca^{2+} decreased by a factor of 5 to 7 within four decades, slightly preceding the d shift by 10 ± 5 years. In contrast, during the cooling event, the dust and Ca^{2+} concentrations increased by a factor of 5 over a period of more than a century, slightly lagging the d shift by 20 ± 10 years.

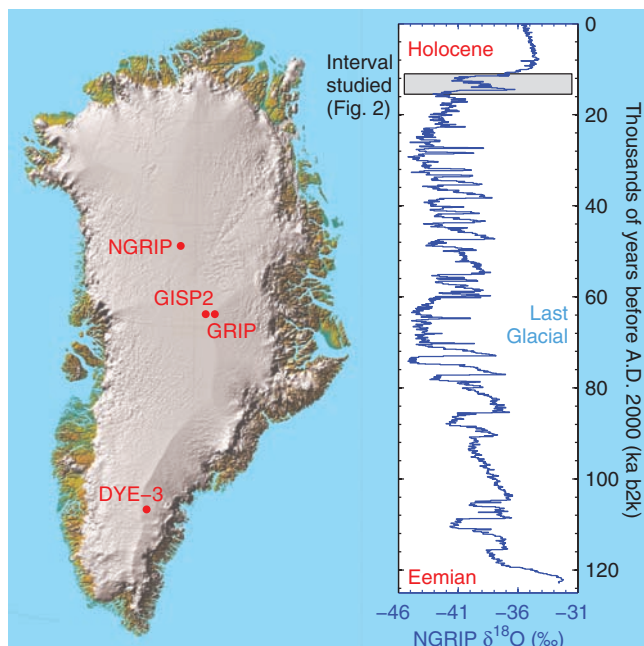
The concentration of Na^+ , which is mainly a marine sea-salt indicator, shows only moderate changes at the transitions as compared with its interannual variability. Changes in sea-ice extent are expected to influence sea-salt export to Greenland through changing the distance to open water

and altering sea-salt aerosol contributions from sea-ice and open-water sources. However, meteorological conditions play an important role in modulating the sea-salt uplift, transport, and deposition on the Greenland ice sheet (29). Although insufficient quantitative understanding of the processes involved is available, the lack of a fast response of the marine sea-salt proxy may be seen as a gradual change in sea ice or as a combination of changes in sea ice and meteorology, compensating for each other to some extent.

This high-resolution study shows a previously unknown sequence of events and gives insights into both the onset and evolution of a rapid climate shift. Our records demonstrate that the last two major warming events followed the same general pattern. During Greenland cold phases, the thermohaline circulation (THC) was reduced, northern sea ice extended far south, and the Intertropical Convergence Zone (ITCZ) was shifted southward, resulting in dry conditions at the low-latitude dust-source regions (22, 30, 31). Meanwhile, southern high latitudes and tropical oceans accumulated heat and underwent gradual warming as reflected in the bipolar seesaw pattern (32, 33), because of a reduction in the North Atlantic overturning circulation. We suggest that this Southern Hemisphere/tropical warming induced first a northward shift of the ITCZ and, when a threshold was reached, an abrupt intensification of the Pacific monsoon. The wetter conditions at the Asian dust-source areas then caused decreased uplift and increased washout of atmospheric dust, leading to the first sign of change in Greenland: decreasing dust and Ca^{2+} concentrations. This reorganization of the tropical atmospheric circulation was followed by a complete reorganization of the mid- to high-latitude atmospheric circulation almost from one year to the next, as identified by the 1-to-3-year transitions in d . Sea ice then started retreating in the North Atlantic, associated with increased advection of atmospheric heat and moisture, as indicated by Greenland changes in $\delta^{18}\text{O}$ and λ (22, 34).

Both abrupt warming events of the last termination are characterized by this sequence of events, even though they occurred at different stages of deglaciation. The 14.7-ka event followed Heinrich event H1 at a time when the ice sheets in the north were still extensive, whereas the north was more deglaciated at 11.7 ka (35), reducing the amount of ice discharge available to change the density of North Atlantic ocean waters and thereby the THC before the warming onset (35). The NGRIP ice core has also revealed that the very first interstadial of the last glacial cycle occurred at the inception of the glacial period 110 ka, before the ice sheets were fully developed and the climate system had cooled to full glacial conditions (1). The detailed sequence of events obtained here for the most recent warming events suggests that the classical bipolar seesaw concept (32) involving the ocean THC reorganization must include the role of abrupt atmospheric circulation changes from the tropics to the high

Fig. 1. (Left) Location of drill sites on the Greenland Ice Sheet: DYE-3 (65.15°N, 43.82°W), GRIP (72.59°N, 37.64°W), GISP2 (72.58°N, 38.46°W), and NGRIP (75.10°N, 42.32°W). (Right) The NGRIP stable water isotope profile ($\delta^{18}\text{O}$) on the GICC05 time scale (1, 2). The zone studied (11.0 to 15.5 ka) is marked with gray shading.



northern latitudes in the onset of abrupt warmings seen in the North Atlantic region.

The cooling at 12.9 ka is characterized by relatively longer transition times for all parameters except for d , and the sequence of events is notably different. In this case, changes in d and $\delta^{18}\text{O}$

precede the dust and Ca^{2+} reactions. The centennial scale change in $\delta^{18}\text{O}$ follows anterior gradual cooling during the Allerød period, probably including gradual buildup of sea ice. Given the generally slow nature of the coolings, the persistent rapid switch of the atmospheric

circulation as recorded by the excess is even more surprising and confirms the potential for extremely abrupt reorganizations of the Arctic atmospheric circulation, whether going from cold to warm or vice versa. The lag and longer duration of the dust and Ca^{2+} responses may be

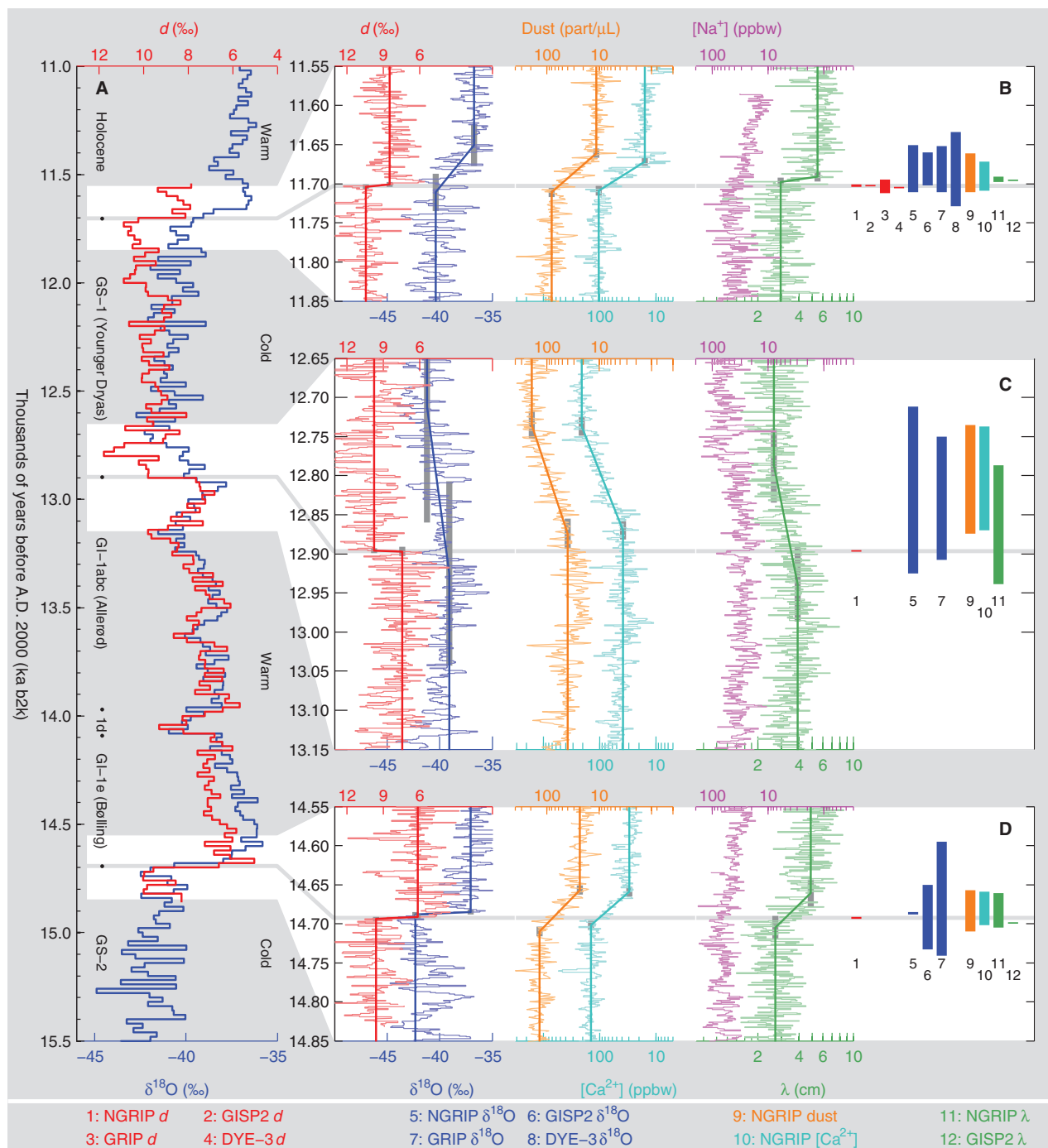


Fig. 2. Multiple-parameter records from the NGRIP ice core 11.0 to 15.5 ka. (A) d (red) and $\delta^{18}\text{O}$ (dark blue) at 20-year resolution over the entire period and details of the transition zones: (B) from GS-1 into the Holocene at 11.7 ka, (C) from GI-1a into GS-1 at 12.9 ka, and (D) from GS-2 into GI-1e at 14.7 ka. [Left part of (B) to (D)] NGRIP records of d (red), and $\delta^{18}\text{O}$ (dark blue) and logarithmic plots of dust content (yellow), calcium concentration ($[\text{Ca}^{2+}]$, light blue), sodium concentration ($[\text{Na}^+]$, purple), and annual layer thickness (λ , green) at annual resolu-

tion. Bold lines show the fitted ramp functions; gray vertical bars represent the 95% (2σ) confidence intervals of the ramp point locations. [Right part of (B) to (D)] Bars representing the locations of the fitted ramp functions for the NGRIP records shown to the left and for the corresponding results obtained using DYE-3, GRIP, and GISP2 data, where these are available at sufficient resolution (see list of records below the figure). See Table 1, SOM methods, and table S2 (15) for additional information on ramp fitting.

due to the inertia of land surfaces drying out and vegetation dying off in the dust-source regions before large fluxes of dust could be reestablished.

The high-resolution records from the NGRIP ice core reveal that polar atmospheric circulation can shift in 1 to 3 years, resulting in decadal- to centennial-scale changes from cold stadials to

warm interstadials/interglacials associated with large Greenland temperature changes of 10 K (6, 20). Neither the magnitude of such shifts nor their abruptness is currently captured by state-of-the-art climate models. We propose a series of events, beginning in the lower latitudes and leading to changes in the ocean and atmosphere, that

reveals for the first time the anatomy of abrupt climate change. Although no large shifts in d can be identified over the course of the Holocene in the Greenland ice cores (36), past warming events now documented at subannual resolution offer important benchmarks with which to test climate models. If we are to be confident in the ability of those models to accurately predict the impacts of future abrupt change, their ability to match what we see in the past is crucial.

Fig. 3. (A to C) d (red) at measured resolution and the fitted ramp curves across the same transitions as shown in Fig. 2, B to D. The mean values over the 150 years before and after the transitions are shown as bold red lines. (Left) To visualize the shifts, the areas within 1 SD from the mean values are shaded light gray. Where the data values are more than 1 SD away from the mean, the zone is colored light blue. (Right) Histograms (gray) of the distribution of the d values in the states before and after the rapid shifts. The mean values are shown as bold red lines. Because of the abruptness of the d shifts, the ramp-fitting method produces results with very small uncertainties. Therefore, we suggest that the d record be used for defining transition points between different climatic episodes, especially for the transitions studied here (15.5 to 11.0 ka) but possibly also for those found in the older part of the NGRIP record (123.0 to 15.5 ka).

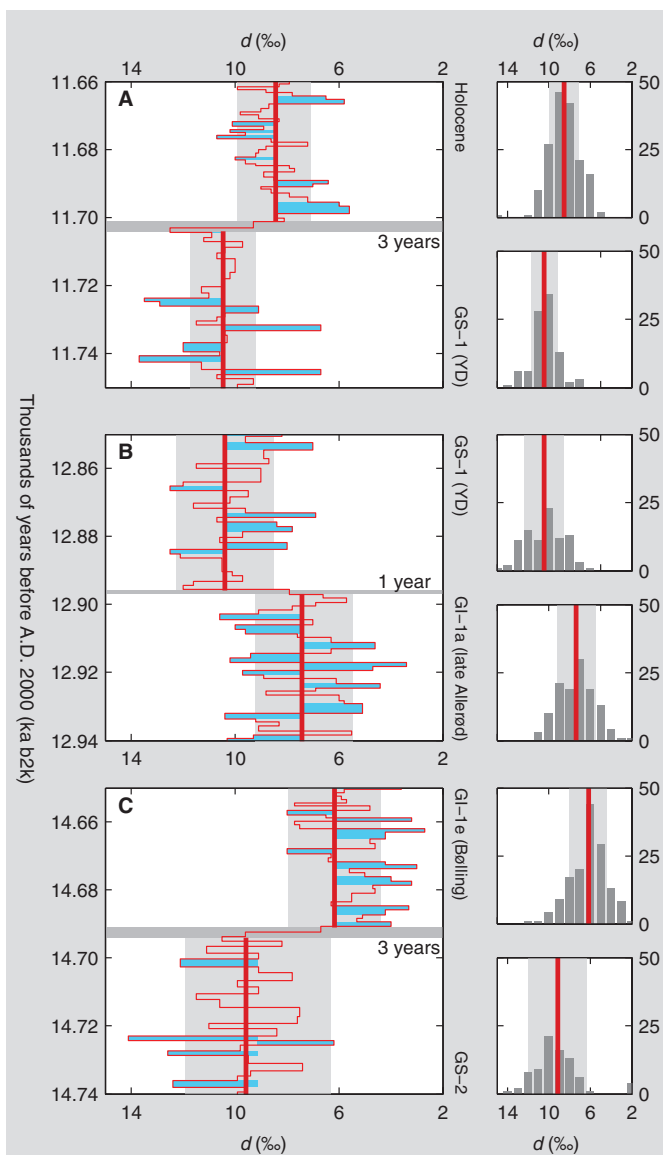


Table 1. Ramp-fitted transition times. Ramp-fitting results (14) for $\delta^{18}\text{O}$, d , dust content, Ca^{2+} , and λ over the three transitions from Greenland Stadial 1 (GS-1) into the Holocene at 11.7 ka, from Greenland Interstadial 1a (GI-1a) into GS-1 at 12.9 ka, and from GS-2 into GI-1e at 14.7 ka. The GICC05 time scale (2), produced by multiple-proxy identification of annual layers using NGRIP impurity records, provides the ages. The timing and standard error of the ramp points are listed at the onset and termination of the transitions. Times are in years before 2000 AD.

Period	$\delta^{18}\text{O}$	d	Dust	Ca^{2+}	λ
Start of Holocene	11,651 ± 13	11,701 ± 1.5	11,661 ± 3.0	11,672 ± 3.0	11,691 ± 3.0
End of GS-1	11,711 ± 12	11,704 ± 1.5	11,711 ± 3.0	11,709 ± 3.0	11,698 ± 3.0
Start of GS-1	12,712 ± 74	12,896 ± 1.5	12,735 ± 8.9	12,737 ± 8.9	12,787 ± 24
End of GI-1a	12,925 ± 59	12,897 ± 3.0	12,874 ± 9.6	12,870 ± 5.9	12,939 ± 24
Start of GI-1e	14,685 ± 1.5	14,691 ± 1.5	14,657 ± 3.0	14,659 ± 3.0	14,661 ± 8.9
End of GS-2	14,688 ± 1.5	14,694 ± 1.5	14,710 ± 3.0	14,702 ± 3.0	14,705 ± 7.4

References and Notes

1. North Greenland Ice Core Project Members, *Nature* **431**, 147 (2004).
2. S. O. Rasmussen *et al.*, *J. Geophys. Res.* **111**, D06102 (2006).
3. R. B. Alley *et al.*, *Science* **299**, 2005 (2003).
4. W. Dansgaard, J. W. C. White, S. J. Johnsen, *Nature* **339**, 532 (1989).
5. J. J. Lowe, M. J. C. Walker, *Reconstructing Quaternary Environments* (Pearson Higher Education, New Jersey, ed. 2, 1997).
6. J. P. Severinghaus, E. J. Brook, *Science* **286**, 930 (1999).
7. W. Dansgaard *et al.*, *Science* **218**, 1273 (1982).
8. S. J. Johnsen *et al.*, *J. Geophys. Res.* **102**, 26397 (1997).
9. P. M. Grootes, M. Stuiver, J. W. C. White, S. J. Johnsen, J. Jouzel, *Nature* **366**, 552 (1993).
10. U. Ruth *et al.*, *Geophys. Res. Lett.* **34**, L03706, 10.1029/2006GL027876 (2007).
11. R. Röthlisberger *et al.*, *Environ. Sci. Technol.* **34**, 338 (2000).
12. M. Bigler, thesis, University of Bern, Switzerland (2004).
13. U. Ruth, D. Wagenbach, J. P. Steffensen, M. Bigler, *J. Geophys. Res.* **108**, 4098 (2003).
14. M. Mudelsee, *Comput. Geosci.* **26**, 293 (2000).
15. Materials and methods are available as supporting material on Science Online.
16. V. Masson-Delmotte *et al.*, *Science* **309**, 118 (2005).
17. W. Dansgaard *et al.*, in *Climatic Processes and Climate Sensitivity*, vol. Maurice Ewing 5, J. E. Hansen, T. Takahashi, Eds. (American Geophysical Union, Washington, DC, 1984), pp. 288–298.
18. J. Jouzel *et al.*, *Quat. Sci. Rev.* **26**, 1 (2007).
19. M. Werner, M. Heimann, G. Hoffmann, *Tellus B Chem. Phys. Meteorol.* **53**, 53 (2001).
20. A. Landais, J. Jouzel, V. Masson-Delmotte, N. Caillon, *C. R. Geosci.* **337**, 947 (2005).
21. S. J. Johnsen *et al.*, *J. Quat. Sci.* **16**, 299 (2001).
22. C. Li, D. S. Battisti, D. P. Schrag, E. Tziperman, *Geophys. Res. Lett.* **32**, L19702, 10.1029/2005GL023492 (2005).
23. S. J. Johnsen, W. Dansgaard, J. W. C. White, *Tellus B Chem. Phys. Meteorol.* **41**, 452 (1989).
24. J. Jouzel *et al.*, *J. Geophys. Res.* **96**, 7495 (1991).
25. D. A. Fisher, *Tellus Ser. B Chem. Phys. Meteorol.* **43**, 401 (1991).
26. M. Winton, *Geophys. Res. Lett.* **33**, L23504 (2006).
27. C. Hillaire-Marcel, A. de Vernal, *Earth Planet. Sci. Lett.* **268**, 143 (2008).
28. A. Svensson, P. E. Biscaye, F. E. Grousset, *J. Geophys. Res.* **105**, 4637 (2000).
29. M. A. Hutterli *et al.*, *Clim. Dyn.*, 10.1007/s00382-006-0211-z (2006).
30. D. W. Lea, D. K. Pak, L. C. Peterson, K. A. Hughen, *Science* **301**, 1361 (2003).
31. J. W. Partin, K. M. Cobb, J. F. Adkins, B. Clark, D. P. Fernandez, *Nature* **449**, 452 (2007).
32. T. F. Stocker, S. J. Johnsen, *Paleoceanography* **18**, 1087 (2003).
33. EPICA Community Members, *Nature* **444**, 195 (2006).
34. J. C. H. Chiang, C. M. Bitz, *Clim. Dyn.* **25**, 10.1007/s00382-005-0040-5 (2005).
35. K. Lambek, T. M. Esat, E.-K. Potter, *Nature* **419**, 199 (2002).
36. V. Masson-Delmotte *et al.*, *J. Geophys. Res.* **110**, D14102 (2005).
37. NGRIP is directed and organized by the Ice and Climate Research Group, Niels Bohr Institute, University of

Downloaded from www.sciencemag.org on May 5, 2010

Copenhagen. It is supported by funding agencies in Denmark (Forskningrådet for Natur og Univers), Belgium (Fonds National de la Recherche Scientifique), France (Institut Polaire Française and Institut National des Science l'Univers/CNRS), Germany (AWI), Iceland (Rannís), Japan (Ministry of Education, Culture, Sports, Science and Technology), Sweden

(Polarforskningssekretariatet), Switzerland (Der Schweizerische Nationalfonds) and the United States (NSF, Office of Polar Programs).

Supporting Online Material
www.sciencemag.org/cgi/content/full/1157707/DC1
Materials and Methods

Tables S1 and S2
Data

12 March 2008; accepted 12 June 2008
Published online 19 June 2008;
10.1126/science.1157707
Include this information when citing this paper.

The Global Stoichiometry of Litter Nitrogen Mineralization

Stefano Manzoni,¹ Robert B. Jackson,² John A. Trofymow,³ Amilcare Porporato^{1*}

Plant residue decomposition and the nutrient release to the soil play a major role in global carbon and nutrient cycling. Although decomposition rates vary strongly with climate, nitrogen immobilization into litter and its release in mineral forms are mainly controlled by the initial chemical composition of the residues. We used a data set of ~2800 observations to show that these global nitrogen-release patterns can be explained by fundamental stoichiometric relationships of decomposer activity. We show how litter quality controls the transition from nitrogen accumulation into the litter to release and alters decomposers' respiration patterns. Our results suggest that decomposers lower their carbon-use efficiency to exploit residues with low initial nitrogen concentration, a strategy used broadly by bacteria and consumers across trophic levels.

Plant residues deposited to the soil are subject to biological degradation (1–3). During this process, litter carbon (C) is respired to CO₂ while providing energy to the decomposers, whereas nutrient concentrations generally increase (4). Nutrients in mineral forms are taken up by the decomposers (immobilized) and thus accumulate in the litter. Typically, net nitrogen (N) release in mineral forms (ammonium and nitrate) from a given plant residue (net mineralization) only occurs after N concentration reaches a critical value (1). Knowledge of this threshold and how it is related to biogeochemical or climatic factors is essential to predict the patterns of nutrient cycling in natural and agricultural settings (4–6), to improve our understanding of ecosystem stoichiometry (7, 8), and to constrain biogeochemical models (9). The biological degradation of litter is mainly carried out by microbial decomposers, including bacteria and fungi, and their grazers, which have higher N:C values compared with most litter types (1). This creates a high N demand, and, even though a considerable fraction of assimilated C is respired, the decomposers often still require some inorganic N uptake during at least the early phases of decomposition. The decomposer N:C and the respiration rate (complementary to the carbon-use efficiency) define the actual nutrient requirement of the decomposers (9–11). Although the decomposer N:C ratios have been observed to be relatively constant across ecosystems and litter types, the causes of patterns of variation in carbon-use efficiency are still unclear.

We analyzed litter decomposition data including the temporal evolution of both carbon and nitrogen, as measured in litterbags left to decompose in field conditions (12) or from chemical analysis of large branches and logs along decomposition chronosequences. On the basis of 55 litter types classified by initial N concentrations ranging from 0.03% to 3% (13), we show that the carbon-use efficiency tends to increase with higher initial substrate N:C ratio, which corresponds to a more-efficient nitrogen use and a less-efficient carbon use for N-poor substrates (i.e., litter with low N concentration and low N:C). In turn, low carbon-use efficiencies allow net mineralization to occur early during decomposition, even in relatively N-poor residues.

The dynamics of net N immobilization, accumulation, and mineralization have been described mathematically with mass balance equations (9, 11, 14). We developed a general set of such equations that allows us to obtain universal analytical curves of N accumulation and release during decomposition, when the decomposer characteristics can be assumed relatively constant in time (13). Specifically, the general expression for the fraction of initial litter nitrogen content, n , as a function of the fraction of remaining carbon content in the litter sample, c , can be written independently of the specific decomposition model as

$$n(c) = c \frac{r_B}{r_{L,0}} + \left(1 - \frac{r_B}{r_{L,0}}\right) c^{\frac{1}{1-e}} \quad (1)$$

where $r_{L,0}$ is the initial litter N:C ratio, r_B is the decomposer biomass N:C, and e is the decomposer carbon-use efficiency (i.e., amount of C in new biomass per unit C decomposed). Thus, the N dynamics are represented in terms of the fraction of remaining litter C content, avoiding any explicit account of the temporal variability of decomposition rates caused by climatic fac-

tors or nutrient limitation. On the basis of data from 15 data sets containing observations at more than 60 sites worldwide (table S1), this universal representation of N immobilization and release curves appears to be valid across diverse terrestrial ecosystems and with different initial litter N:C values.

During decomposition, the fraction of remaining N and lost C move along the curves from left to right at a speed dictated by biogeochemical and environmental conditions (Fig. 1). All the curves show slower N loss than C loss, meaning that N tends to accumulate, and the N:C ratio of the litter increases throughout decomposition. Where the curves increase with respect to the initial condition, not only is N retained more efficiently than C, but net immobilization occurs. At the point on each curve where n is maximal, immobilization ends and net mineralization begins. Conversely, if the curve decreases monotonically there is no initial net immobilization, as in Fig. 1, A and B. The maximum of the N release curve thus corresponds to the litter critical N concentration, which can be expressed analytically in terms of N:C ratio as a function of the decomposer characteristics, $r_{CR} = e r_B$ (9, 10). In general, the lower r_{CR} is, the earlier N release occurs, even in N-poor residues. Moreover, when $r_{CR} < r_{L,0}$, net release occurs from the beginning of decomposition. Conversely, if r_{CR} is high, large amounts of mineral N have to be immobilized to increase the litter N concentration to its critical value.

The litter decomposition observations and Eq. 1 can be used to study the patterns of variation of the litter r_{CR} and decomposer characteristics. Using the analytical N release curve provides a theoretical underpinning to previous estimates of the onset of mineralization based on regressions of field observations (4, 15) and offers robust estimates of r_{CR} and the decomposer parameters, e and r_B . In particular, r_B does not vary systematically along gradients of organic matter and litter N:C and typically remains in the range of 0.07 to 0.2 [or C:N between 5 and 15 (7, 16, 17)]. We thus assumed an average value of $r_B = 0.1$ and fitted the remaining free parameter, e , for each litter type (13). For given values of r_B and e and applying a nonlinear transformation of Eq. 1, all observations of litter C and N content collapse well onto a single 1:1 curve (Fig. 2 and fig. S1), showing that the variation of e alone explains most of the variability in the data.

We assessed how r_{CR} and e , which are simply proportional when r_B is a constant, respond to changes in climatic variables and initial litter conditions. Parton *et al.* (18) and Moore *et al.* (15) noted that the N release patterns observed in two

¹Civil and Environmental Engineering Department, Duke University, Durham, NC 27708, USA. ²Department of Biology and Nicholas School of the Environment, Duke University, Durham, NC 27708, USA. ³Canadian Forest Service, Pacific Forestry Centre, Victoria, BC V8Z 1M5, Canada.

*To whom correspondence should be addressed. E-mail: amilcare@duke.edu